We are IntechOpen,
the world's leading publisher of
Open Access books
Built by scientists, for scientists

6,900
Open access books available

186,000
International authors and editors

200M
Downloads

Our authors are among the

154
Countries delivered to

TOP 1%
most cited scientists

12.2%
Contributors from top 500 universities

BOOK CITATION INDEX
CLARIVATE ANALYTICS
INDEXED

WEB OF SCIENCE™

Selection of our books indexed in the Book Citation Index
in Web of Science™ Core Collection (BKCI)

Interested in publishing with us?
Contact book.department@intechopen.com

Numbers displayed above are based on latest data collected.
For more information visit www.intechopen.com

Determination of Optimal Parameters and Feasibility for Imaging of Epileptic Seizures by Electrical Impedance Tomography: A Modelling Study Using a Realistic Finite Element Model of the Head

L. Fabrizi[1], L. Horesh[1], J. F. Perez-Juste Abascal, A. McEwan[3],
O. Gilad[1], R. Bayford[2] and D. S. Holder[1]
[1]Department of Medical Physics and Bioengineering, University College London,
[2]Department of Natural Science, Middlesex University, London,
[3]School of Electrical and Information Engineering, The University of Sydney,
[1,2]UK
[3]Australia

1. Introduction

One potentially powerful application of Electrical Impedance Tomography (EIT) lies in the detection of the source of epileptic seizures in the brain (Holder, 2005). Many patients with epilepsy can be treated with drugs, but surgical resection of the abnormal region which produces seizures may be the only option in severe cases (Engel, Jr., 1993; Rosenow and Luders, 2001). For these, EIT could be used to provide continuous imaging over days while the subject is observed on a ward and so could, uniquely, provide images of conductivity changes related to increased blood volume or cell swelling in the onset zone of the brain where the seizure starts. If successful, this would provide imaging evidence not possible with any other method and would obviate the need in some difficult cases for invasive investigation with intracranial electrodes (Fabrizi et al., 2006).

It has already been shown that impedance increases locally in the brain by 3-12% at 1kHz up to 22% at 50 Hz during induced epileptic seizures (Elazar et al., 1966; Fox et al., 2004; VAN HARREVELD and Shade, 1962). Resistance changes of 5.5-7.1% associated with focal and generalized seizures have been imaged with EIT using a ring of electrodes placed on the exposed cortex of rabbits at 51 kHz (Rao, 2000). It therefore seems plausible that these changes are large enough to enable EIT to produce images of conductivity variations of clinical interest. Nevertheless, in a first pilot study in humans, it was not possible to measure reproducible boundary voltage changes during seizures as they were reaching 1-54% (Fabrizi et al., 2006). The most probable explanation was that true scalp voltage changes due to cerebral seizure were obscured by movement artefacts. However it was not clear whether even in ideal conditions it would have been possible to obtain informative tomographic images.

Therefore it is important to understand what are the EIT hardware and recording system requirements that would maximise the chance of detecting reliable changes associated with

an epileptic seizure. In this chapter, computer simulations of the problem are used to suggest the best recording parameters, set a specification for hardware accuracy, and, finally, assess whether EIT imaging of seizures appears feasible with the suggested optimal arrangement in ideal conditions.

1.1 Experimental design

The complex boundary voltages on the scalp were calculated by solving the forward problem for a realistic 3D Finite Element Model (FEM) of the human head under normal conditions and during focal epileptic seizures. The FEM comprised regions of grey and white matter, cerebrospinal fluid (CSF), skull, scalp and eyes. The complex conductivities were extrapolated from the literature at 7 frequencies between 5Hz and 4MHz, as this is the available range in present EIT systems (McEwan et al., 2006; Oh et al., 2005). Four brain regions, which are common sources of epileptic activity, were chosen as the epileptic onset areas. The detection from scalp measurements was of increasing difficulty, as they decreased in volume and increased in depth. For simplicity, the tissues were all assumed to be isotropic.

Two different current level patterns with respect to frequency were considered, in order to choose the best measuring combination of frequencies or single frequency: (i) a uniform level of 100µA across the whole spectrum; (ii) an increasing pattern with frequency, as the International Electrotechnical Commission IEC601 standard specifies a 'patient auxiliary current' limit of 100µA from 0.1 Hz to 1 kHz; then $100*f$ µA from 1 kHz to 100 kHz where f is the frequency in kHz; then 10 mA above 100 kHz.

To assess whether the voltage changes obtained in the simulation were large enough to provide clinically useful EIT images, images after adding random noise of 0.3-0.4% to the simulated boundary voltages were reconstructed. For the reconstruction, 50 kHz simulated current was adopted, as findings from the previous section predicted that it would give the highest signal-to-noise ratio (SNR).

Because a temporal resolution of 1 sec is needed to record epileptic seizures, temporal averaging could be considered in order to enhance the SNR.. Different EIT data recording strategies allow different acquisition speeds and therefore time averaging capabilities. The recording strategies to consider are: a) Serial – a single impedance measuring circuit with a multiplexer; b) Semi-parallel – multiple parallel recording but a single current source which is multiplexed between different electrode pairs or c) Fully-parallel – multiple simultaneous current injection and record. The degree of averaging can be estimated as follows: for 31 electrodes, the reconstruction algorithm usually employed in EIT brain imaging has 258 electrode combinations, with 21 different injection pairs. If two periods are sufficient for each measurement and 1 µs is need for the combination switching, the number of frames n which can be averaged in 1 second is 1/(2*258*(1/f+1e-6)) for a serial system, 1/(2*21*(1/f+1e-6)) for a semi-parallel system and f/2 for a fully-parallel system, where f is the measuring frequency (Table 1). The noise reduction is given by √n.

System Type	Current Frequency	
	50 Hz	50 kHz
Serial	no (no)	185 (10x)
Semi-parallel	2.4 (no)	2268 (34x)
Fully-parallel	50 (5x)	50k (158x)

Table 1. Number of frames which can be averaged in 1 second with serial, semi-parallel and fully-parallel systems (resulting noise reduction factor)

2. Methods

2. Impedance properties of tissues in the head
2.1 Impedance values for resting conditions

The conductivity values were obtained with a cubic interpolation between data points taken from the literature at available frequencies. Data collected from tissues as close as possible to living human tissue in the frequency range 5Hz-4MHz were considered. If the frequency range was only partially covered, data from different studies were integrated. Data obtained at body temperature were used when available, otherwise a linear correction of +2 %/oC was applied (Foster and Schwan, 1989). Four-terminal measurements were preferred over two-terminal measurements.

The model used in this chapter was isotropic and homogeneous. Mean representative conductivity values for anisotropic tissues such as scalp, skull and white matter were adopted.

2.2 Scalp

The scalp is the soft tissue that envelops the skull. It comprises skin, connective tissue (superficial fascia), epicranial aponeurosis and epicranius. During EIT experiments, the stratum corneum of the skin is often removed by abrasion. As the authors were not aware of any validated direct measurements of scalp conductivity at the time of writing, they approximated it as a homogenous layer of skeletal muscle. Conductivity was therefore estimated from values for excised bovine paravertebral muscle at body temperature, taking into account muscle anisotropy at 10 Hz-10 MHz (Gabriel et al., 1996a). Considering that muscle fibres in the scalp are parallel to the head surface and to the skull, the final representative scalp conductivity was considered as 2/3 transverse and 1/3 longitudinal that of the muscle, as the current may cross the fibres in the longitudinal or transverse direction (Horesh, 2006).

2.3 Skull

The skull comprises a trabecular layer embedded in two cortical layers. The representative skull conductivity was considered as 2/3 that of cortical bone and 1/3 that of trabecular to represent this composition. Cortical and trabecular bone are anisotropic; unfortunately, no studies which account for this appear to have been performed over the frequency range of interest. Cortical bone admittivity has been measured on rat femur freshly excised over a frequency range of 10 Hz-100 MHz at body temperature without considering anisotropy (Kosterich et al., 1983). Trabecular bone was represented using measurements on frozen cancellous bovine femur samples (Sierpowska et al., 2003) defrosted at room temperature just before the measurements, which were conducted between 20 Hz and 5 MHz. Human trabecular bone was found to be about twice more conductive than bovine under similar experiment conditions (Sierpowska et al., 2005), so the real part of the conductivity was doubled and increased by 30% to adjust a recording temperature of 22 to 37 °C.

2.4 Cerebrospinal fluid (CSF)

CSF is an ionic fluid with high conductivity and null permittivity. The former was almost constant between 10 Hz and 10 kHz for human CSF at body temperature (Baumann et al., 1997). As CSF is a purely resistive medium, the mean of the values below 10 kHz was taken to be constant up to 4 MHz.

2.5 Grey matter

Grey matter mainly comprises nerve cell bodies and their branches, a small proportion of myelinated axons and glial cells; its structure is essentially isotropic. In-vivo measurement in humans have been conducted at 50 kHz (Latikka et al., 2001), but the admittivity of bovine tissue in-vitro was measured between 10 Hz and 20 MHz (Gabriel et al., 1996a). These data were translated according to the Lattika recordings at 50 kHz.

2.6 White matter

White matter mainly comprises myelinated nerve axons, which have different longitudinal and transverse conductivity, and is anisotropic. Since the nerve fibres are randomly oriented, the white matter has been considered to have an equivalent volume of 1/3 of fibres longitudinal to the current path and 2/3 transverse (Ranck, Jr., 1963). The conductivity of a bundle of parallel axons was measured in the two directions in-vivo in the dorsal column of cats between 5 Hz and 50 kHz (Ranck, Jr. and BEMENT, 1965). An averaged conductivity (1/3 longitudinal + 2/3 transverse) was calculated as representative of the white matter. The conductivity of in-vitro bovine tissue has been measured between 10 Hz and 20 MHz (Gabriel et al., 1996a). These data were translated according to the mean difference from the spectrum obtained from Ranck and Bement recordings for the overlapping frequency range and employed in the model.

2.7 Eyes

The eye is a complex ensemble of structures, whose admittivities have been measured separately. Only the cornea, lens, retina, sclera, vitreous and aqueous humours compartments were considered; the other parts of the eye are physically small and their contribution was discounted. The volume of each compartment was estimated from the images on http://www.discoveryfund.org/anatomyoftheeye.html. Due to lack of information through our frequency range, the admittivities extrapolated between 10 Hz and 100 GHz with a model simulating four Cole-Cole type dispersions were employed in the model (Gabriel et al., 1996b). The admittivity of retina was assumed to be equal to that of cornea, since they were similar between 1 MHz and 10 MHz (Gabriel et al., 1996a) and that of aqueous humour was assumed equal to that of vitreous humour, since they were similar between 5 Hz and 2 kHz (Lindenblatt and Silny, 2001).

2.8 Values employed in the model

The real part of the conductivities of the tissues is about 1 order of magnitude larger than the imaginary part (Fig. 1; Table 2).

2.9 Conductivity changes due to focal epilepsy

Published data on impedance changes during seizures are discontinuous over the frequency range considered in this chapter. Impedance changes during spreading depression (SD) were therefore considered to integrate these data. SD has already been used as a model for epilepsy since it has similar impedance characteristics (Boone et al., 1994) and probably is due to the same cell processes (Leao, 1944).

The real and imaginary component of the resistivity have been measured separately in anesthetized rabbits during SD at frequencies between 5Hz and 50kHz (Ranck Jr, 1964). The change in conductivity and dielectric constant have also been recorded in

anesthetized rats at frequencies between 300 kHz and 100 MHz (Yoon et al., 1999). These measurements were converted in specific conductivity and scaled to take into account differences between epilepsy and SD, such as lower extracellular space shrinkage (Lux et al., 1986). Resistance changes of 9.5±1.4% during focal epileptic seizures at 47 kHz were measured locally in anesthetized rabbits (Rao, 2000). The ratio between this change and the change in the real part of the resistivity in SD at 50 kHz (Ranck's measurement closer to 47 kHz) was used to transform changes due to SD to changes due to epilepsy. Since the basic mechanisms underlying both SD and epilepsy are likely to be identical (VAN HARREVELD and Shade, 1962) the changes in cell membrane could be considered the same in both conditions. The main difference between them is then the different extent of cell swelling. When the extracellular space shrinks, more current is likely to go through the cells (Ranck Jr, 1964). Since cell swelling is less in epilepsy, the variation in the real and imaginary component of the resistivity would be reduced to the same extent in epilepsy with respect to SD; the same conversion was used also at frequencies different from 50 kHz. The predictions from these assumptions were similar to those found experimentally by Elazar et al. (Elazar et al., 1966) and Fox et al. (Fox et al., 2004).
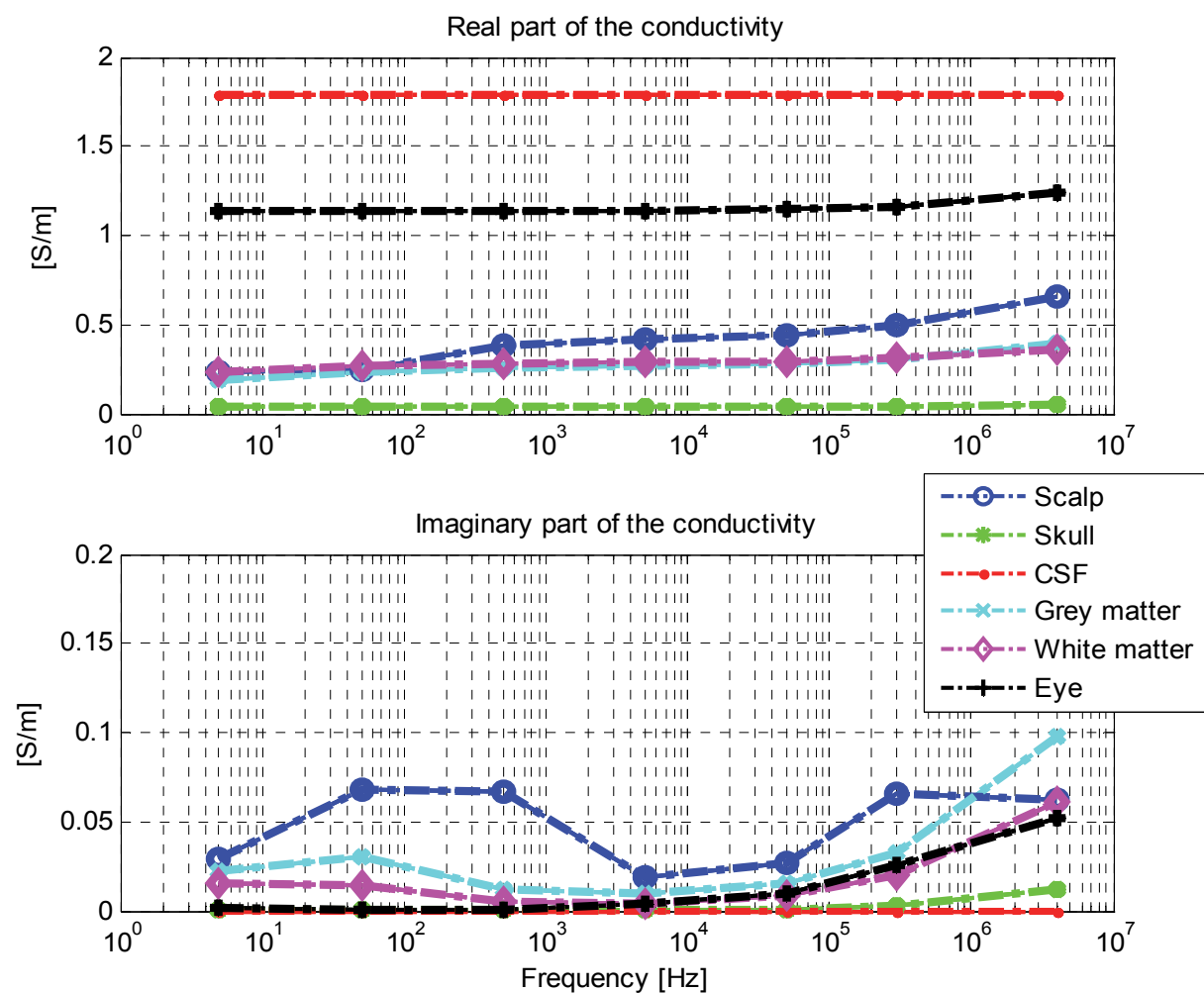

Fig. 1. Estimated conductivity spectra of the tissues in the adult human head employed in this study.

Tissue		Frequency						
		5Hz	50Hz	500Hz	5kHz	50kHz	300kHz	4MHz
Scalp	Re (S/m)	0.235	0.247	0.382	0.419	0.437	0.503	0.653
	Im (S/m)	0.029	0.067	0.067	0.019	0.027	0.066	0.062
Skull	Re (S/m)	0.037	0.037	0.038	0.038	0.039	0.041	0.047
	Im (S/m)	5e-4	4e-4	1e-4	2e-4	0.001	0.002	0.012
CSF	Re (S/m)	1.793	1.793	1.793	1.793	1.793	1.793	1.793
	Im (S/m)	0	0	0	0	0	0	0
Grey matter	Re (S/m)	0.185	0.232	0.259	0.270	0.285	0.306	0.391
	Im (S/m)	0.023	0.030	0.012	0.009	0.016	0.033	0.098
White matter	Re (S/m)	0.238	0.273	0.283	0.288	0.296	0.309	0.361
	Im (S/m)	0.016	0.014	0.005	0.004	0.009	0.019	0.062
Eyes	Re (S/m)	1.136	1.139	1.139	1.142	1.150	1.163	1.238
	Im (S/m)	0.002	0.001	0.001	0.004	0.009	0.026	0.052

Table 2. Estimated values of the real (Re) and imaginary (Im) part of the conductivity spectra of the tissues in the adult human head employed in this study in the frequency range 5Hz-4MHz.

The imaginary part of the conductivity of the grey matter has a larger proportional change than the real part, but its absolute change is smaller (Fig. 2).
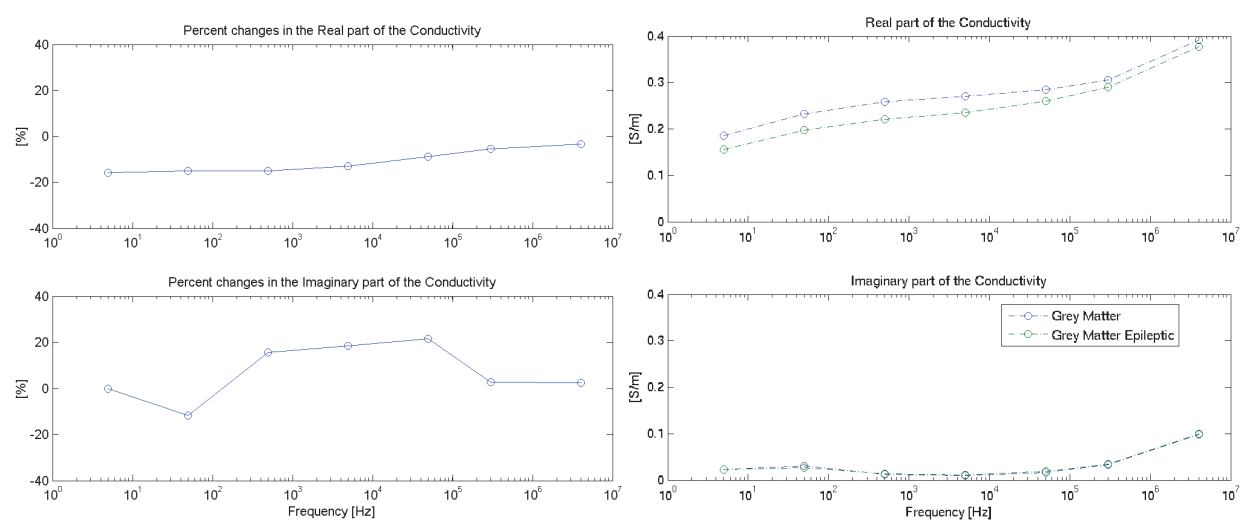

Fig. 2. Estimated conductivity proportional (left) and absolute (right) changes due to focal epilepsy.

3. Methods

3.1 Forward problem and 3D Finite Element Model

In order to determine the boundary voltage changes, the complex forward problem was solved for a realistic 3D Finite Element Model of the human head. The model was obtained using a modified version of EIDORS-3D Toolkit, which includes a finite element field solver (Polydorides and Lionheart, 2002) and a realistic head shaped multi-compartment mesh of 53000 elements generated with I-DEAS software (Tizzard et al., 2005). The compartments included scalp, skull, CSF, white and grey matter and eyes. Thirty-one electrodes and one

ground, 10 mm in diameter, were placed in a modified 10-20 system on the scalp. A frequency-dependent contact resistance, obtained experimentally, was included in the model; it decreased from 3 kΩ at 5 Hz to 250Ω at 4 MHz.

The forward problem was solved at 5 Hz, 50 Hz, 500 Hz, 5 kHz, 50 kHz, 300 kHz, and 4 MHz. In each case, the value of the complex conductivity at that frequency was assigned to each compartment. The forward problem was first solved for brain under normal conditions. Then it was solved using the same mesh with modification of the grey matter conductivity for four possible epileptic regions: the lateral temporal lobe, the parahippocampus and hippocampus together, the parahippocampus alone and the hippocampus alone (Fig. 3). The temporal lobe was represented as a disc of 18 cm3 close to the surface, the parahippocampus as a prism with triangular base of 6 cm3 and the hippocampus as a cylinder of 2.5 cm3 deep in the brain. Data from the simulations were obtained from all 94395 possible non-equivalent electrode combinations, according to symmetry and reciprocity principles. No potential differences were calculated from electrode pairs containing current carrying electrodes.
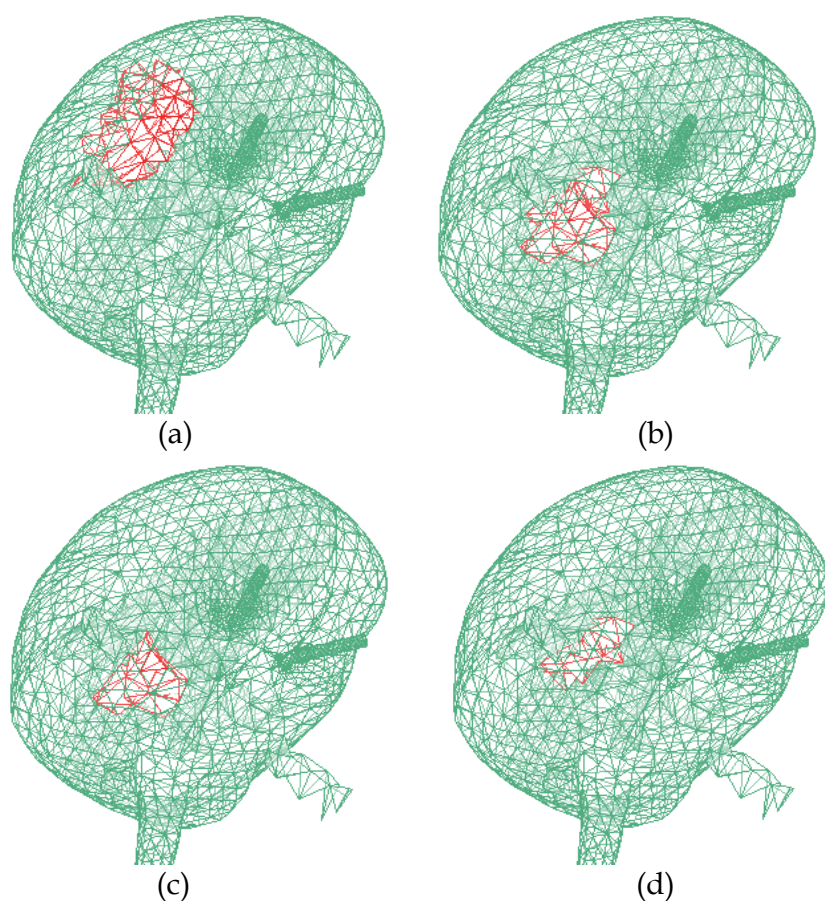

Fig. 3. Focal seizure areas: (a) right lateral temporal lobe; (b) right hippocampus and parahippocampus; (c) right parahippocampus; (d) right hippocampus.

3.2 Boundary voltage analysis method

The complex boundary voltages obtained from all the electrode combinations with a current of 100 µA were considered and the same analysis was conducted separately on the real and imaginary part. Combinations with a low amplitude which could not be accurately measured or

likely to be obscured by noise – less than 0.1 µV for changes during seizures or 100 µV for standing boundary voltages under normal conditions – were eliminated from further investigation for each frequency. The average of the highest 1% of these changes was taken as a representative index together with the corresponding mean absolute change across frequencies. A theoretical advantage existed if greater currents were injected at higher frequencies according to safety standards. To examine this, the effect of greater injected current was simulated by multiplication of boundary voltages, since these are linearly related to injected current with the employed forward problem. The boundary voltages at 5 kHz and 50 kHz were multiplied by $(100*f)\mu A/100\mu A$ and the boundary voltages at 300 kHz and 4 MHz by $10mA/100\mu A$. Since the measured voltages would be greater, the gain of the measuring amplifiers would have needed to be decreased to avoid saturation. To take this into account, combinations with less than 1 µV on the boundary voltage changes during seizures or 1 mV on the standing boundary voltages under normal conditions were eliminated from further investigation for each frequency.

3.3 Image reconstruction

Reporting of the greatest 1% of voltage changes is a simple guide to peak changes. In order to examine whether the predicted changes would translate into clinically useful images, images of the above perturbations were reconstructed using the potential changes obtained from the simulation of a polar injection protocol of 258 electrode combinations with a current of 5 mA at 50 kHz. Random noise with RMS of 0.35% and of 20% was added respectively to the real and imaginary part of the boundary voltages before reconstruction. This noise level was that present on the boundary voltages measured on a cylindrical saline tank with stainless steel electrodes (McEwan et al., 2006). To simulate the possibility of noise reduction with averaging, the noise was decreased 10, 34 or 158 times for serial, semi-parallel or fully parallel systems respectively (Table 1). The linear inverse problem was solved using a complex sensitivity matrix pseudo-inverted by truncated singular value decomposition (Bagshaw et al., 2003), with a fixed truncation level of 10^{-3} of the magnitude of the largest singular value, employing the same mesh of the forward problem.

4. Results

4.1 Simulated boundary voltage changes during seizures with 100µA applied at all frequencies

4.1.1 Real part

The top 1% of changes was 0.77%(1.45µV) at 5-50 Hz falling to 0.12%(0.2µV) at 4 MHz for a seizure in the temporal lobe. It decreased with depth of seizure site to 0.05%(0.13µV) at 5 Hz for a seizure in the hippocampus falling to 0%(0µV) at 4 MHz (Fig. 4, Table 3).

Seizure Focus	Voltage Changes	
	Real	Imaginary
Temporal	0.77%(1.45µV) - 0.77%(1.35µV)	0.48%(0.56µV) - 0.44%(0.57µV)
Para+Hippo	0.15%(0.25µV) - 0.16%(0.24µV)	0.12%(0.15µV) - 0.1%(0.14µV)
Parahippocampus	0.1%(0.16µV) - 0.1%(0.16µV)	0.03%(0.05µV) - 0.03%(0.05µV)
Hippocampus	0.05%(0.13µV) - 0.05%(0.13µV)	0% - 0%

Table 3. Averages of the highest 1% changes at 5Hz - 50Hz when the current level is kept constant across frequency
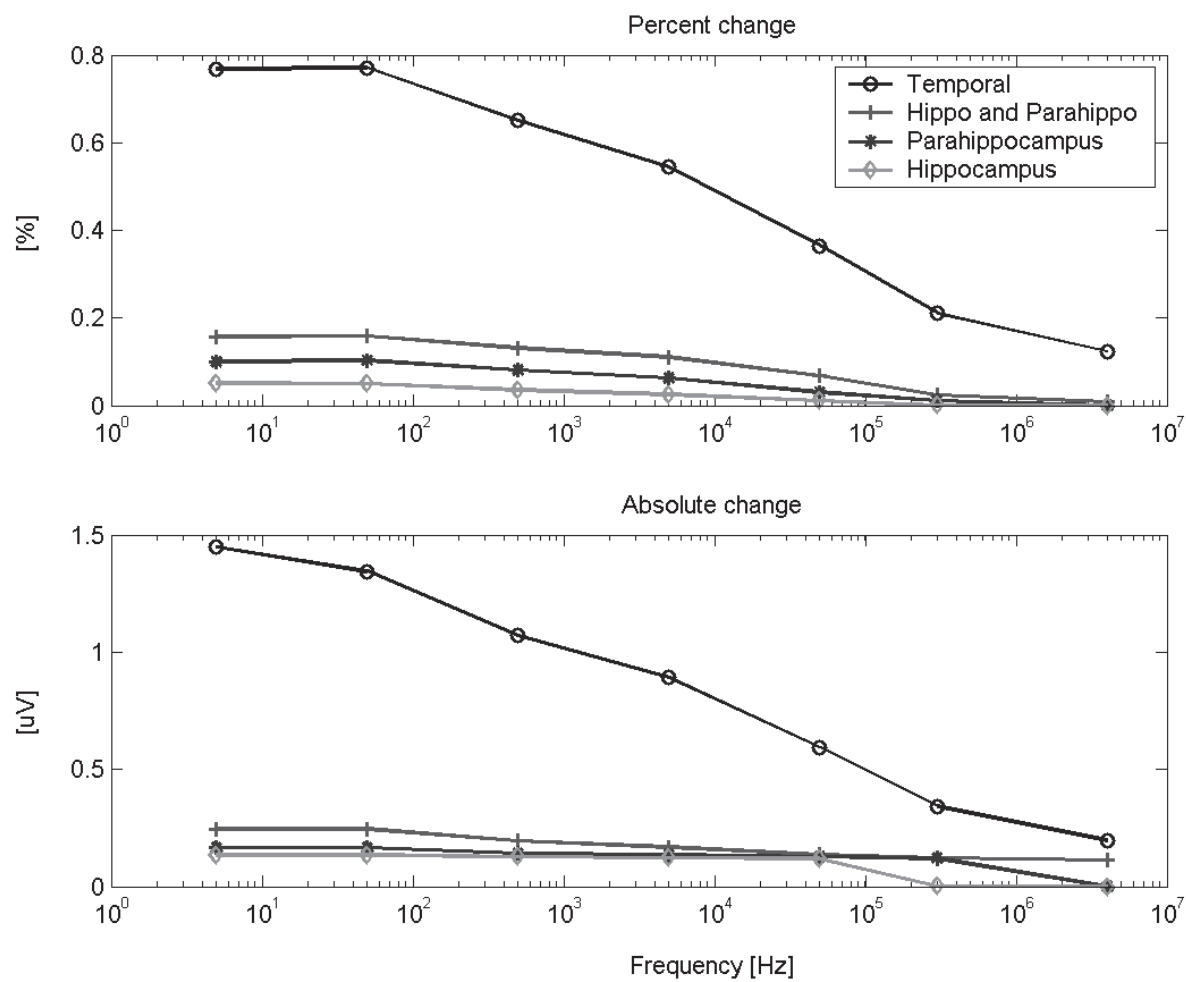
Fig. 4. Average of the largest 1% percent changes

The proportion of electrode combinations with measurable signal increased with the increase of the size of the epileptic region and its proximity to the surface (Table 4).

Seizure Focus	Current Frequency						
	5 Hz	50 Hz	500 Hz	5 kHz	50 kHz	300 kHz	4 MHz
Temporal	79.00	78.70	76.66	74.00	66.75	53.19	35.16
Para+Hippo	56.37	56.34	51.28	45.47	31.61	13.15	1.37
Parahippocampus	41.63	41.68	35.55	29.36	16.18	3.60	0.00
Hippocampus	23.84	23.59	17.90	12.79	4.03	0.02	0.00

Table 4. Percentage of electrode combinations which measure a voltage under normal conditions larger than 100 µV and a change larger 0.1 µV during seizures.

4.1.2 Imaginary part

The top 1% of changes was 0.48-0.44%(0.56-0.54µV) at 5-50 Hz falling to 0%(0µV) at 5 kHz for a seizure in the temporal lobe. It fell to 0%(0µV) at all frequencies for a seizure in the hippocampus (Fig. 5, Table 3).
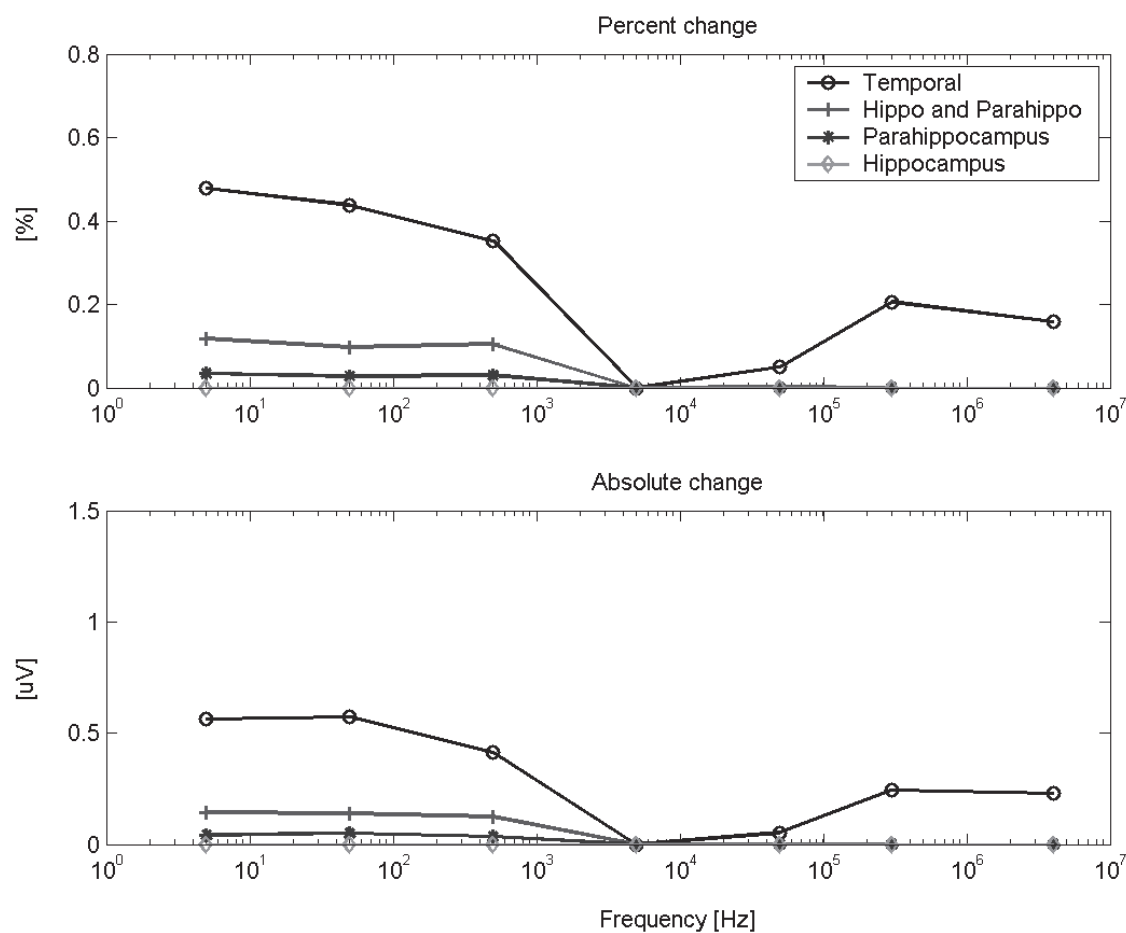
Fig. 5. Average of the largest 1% percent changes

The proportion of electrode combinations with measurable signal was lower than in the real part (Table 5).

Seizure Focus	Current Frequency						
	5 Hz	50 Hz	500 Hz	5 kHz	50 kHz	300 kHz	4 MHz
Temporal	2.36	3.63	1.50	0.00	0.19	4.22	11.40
Para+Hippo	1.03	1.45	0.91	0.00	0.01	0.00	0.00
Parahippocampus	0.39	0.45	0.32	0.00	0.00	0.00	0.00
Hippocampus	0.00	0.00	0.00	0.00	0.00	0.00	0.00

Table 5. Percentage of electrode combinations which measure a voltage under normal conditions larger than 100 μV and a change larger 0.1 μV during seizures.

4.2 Boundary voltage changes during seizures using higher current at high frequencies
4.2.1 Real part

The top 1% of changes was 0.26%(3.4μV) at 500 Hz increasing to 0.97%(21μV) at 50 kHz for a seizure in the temporal lobe. It was 0% (0μV) at 500 Hz increasing to 0.06%(1.8μV) at 50 kHz for a seizure in the hippocampus (Fig. 6, Table 6).
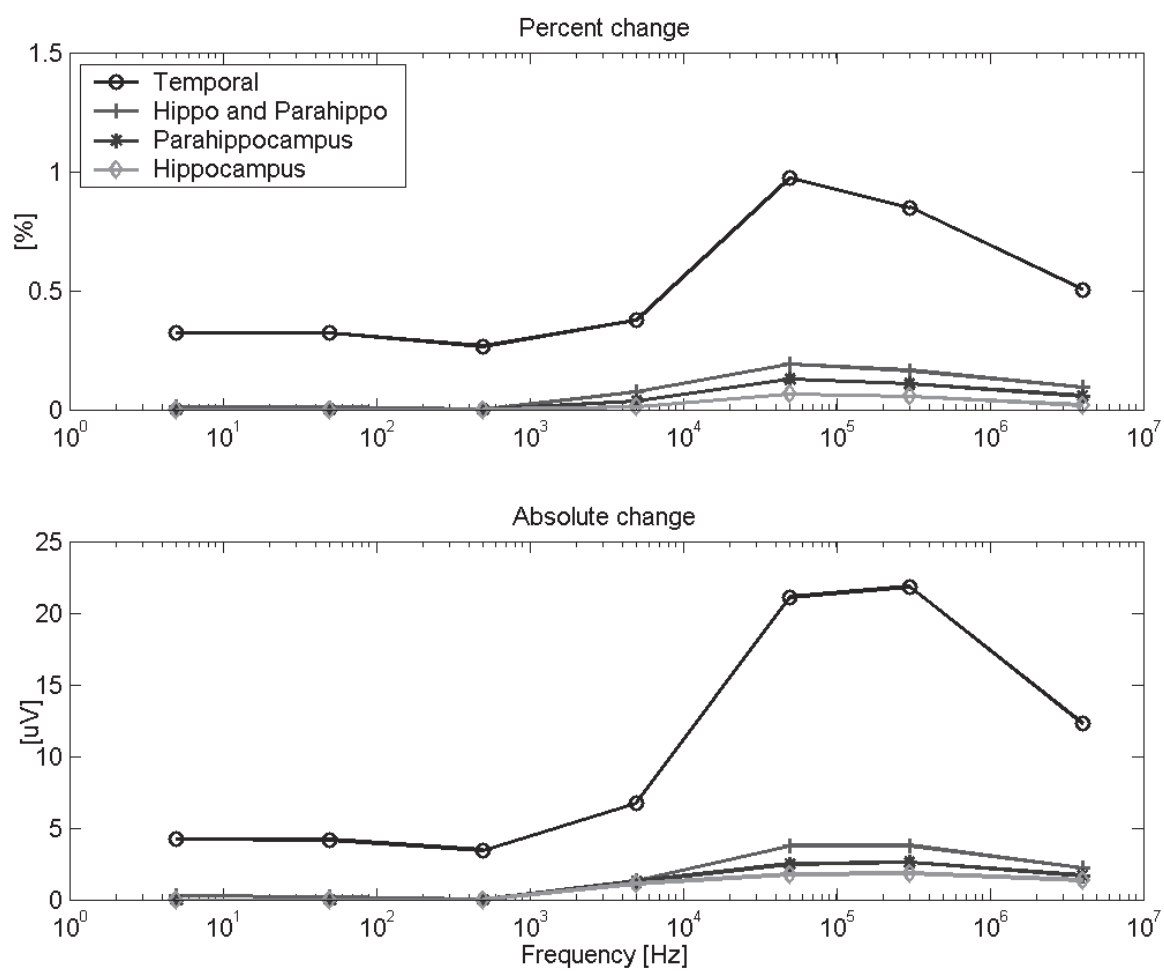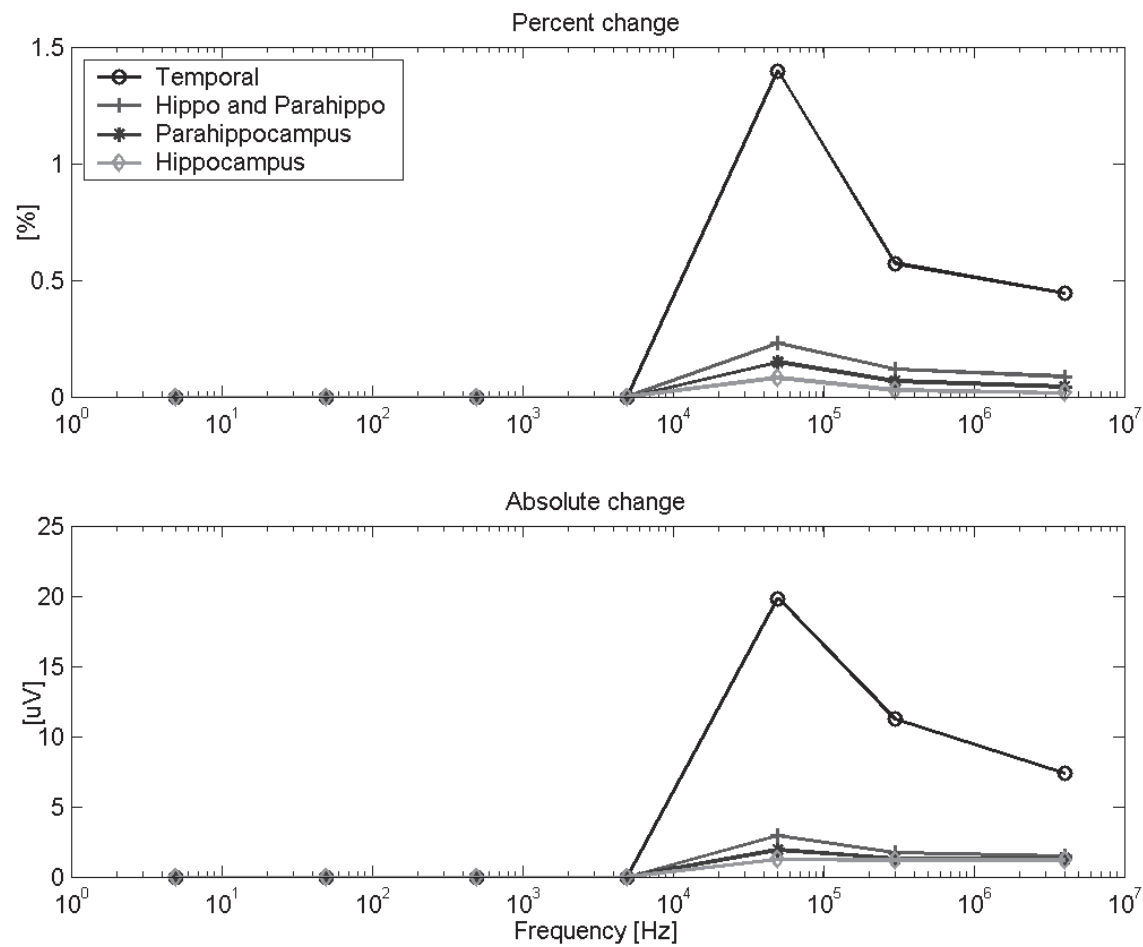
Fig. 6. Average of the largest 1% percent changes

The proportion of electrode combinations with measurable signal increased with the increase of the size of the epileptic region, its proximity to the surface and generally with the increase of the measuring frequency peaking between 50 and 300 kHz before falling at 4MHz (Table 7).

Seizure Focus	Voltage Changes	
	Real	Imaginary
Temporal	0.97%(21.1μV)	1.4%(19.8μV)
Para+Hippo	0.19%(3.75μV)	0.23%(2.9μV)
Parahippocampus	0.12%(2.5μV)	0.15%(1.9μV)
Hippocampus	0.06%(1.75μV)	0.08%(1.2μV)

Table 6. Averages of the highest 1% changes at 50 kHz when the current level conformed to the IEC601 standard

Seizure Focus	Current Frequency						
	5 Hz	50 Hz	500 Hz	5 kHz	50 kHz	300 kHz	4 MHz
Temporal	15.74	15.08	12.89	55.65	92.31	93.94	89.50
Para+Hippo	0.26	0.19	0.00	21.60	79.30	82.12	68.75
Parahippocampus	0.00	0.00	0.00	8.57	69.39	72.88	54.38
Hippocampus	0.00	0.00	0.00	1.09	53.75	58.42	36.02

Table 7. Percentage of electrode combinations which measure a voltage under normal conditions larger than 1 mV and a change larger 1 µV during seizures.

4.2.2 Imaginary part

The top 1% of changes was 0%(0µV) at 500 Hz and below increasing to 1.39%(20µV) at 50 kHz for a seizure in the temporal lobe. It was 0% (0µV) at 500 Hz and below increasing to 0.08%(1.2µV) at 50 kHz for a seizure in the hippocampus (Fig. 7, Table 6).

Fig. 7. Average of the largest 1% percent changes

At low frequencies, no electrode combinations had a measurable signal and the overall amount increases with the increase of the frequency (Table 8).

Seizure Focus	Current Frequency						
	5 Hz	50 Hz	500 Hz	5 kHz	50 kHz	300 kHz	4 MHz
Temporal	0.00	0.00	0.00	0.00	35.52	64.93	74.20
Para+Hippo	0.00	0.00	0.00	0.00	23.61	37.72	43.28
Parahippocampus	0.00	0.00	.0.00	0.00	15.46	22.22	26.27
Hippocampus	0.00	0.00	0.00	0.00	5.56	8.14	10.42

Table 8. Percentage of electrode combinations which measure a voltage under normal conditions larger than 1 mV and a change larger 1 μV during seizures.

4.3 Images reconstructed after addition of noise to simulated boundary voltages

Images of the real part in which a clear change occurred at the site of simulated seizure could be observed for all averaging cases for temporal lobe seizures. For the other three regions, this was only the case for fully parallel systems, which permitted the greatest degree of averaging. For imaginary component images, such accurate images could only be observed for temporal and combined hippocampal and parahippocampal seizure regions for the parallel injection and recording case (Fig. 8-Fig. 11).

Fig. 8. Temporal lobe seizure. In this and the following figures, columns indicate simulated seizure region (1), reconstruction without noise (2), reconstruction with noise for serial (3), semi-parallel (4) and fully parallel (5) systems. Slices are shown from top of the head (top) to bottom (bottom). The colour bar indicates percentage impedance change. Real and imaginary changes are shown on the left and right respectively.
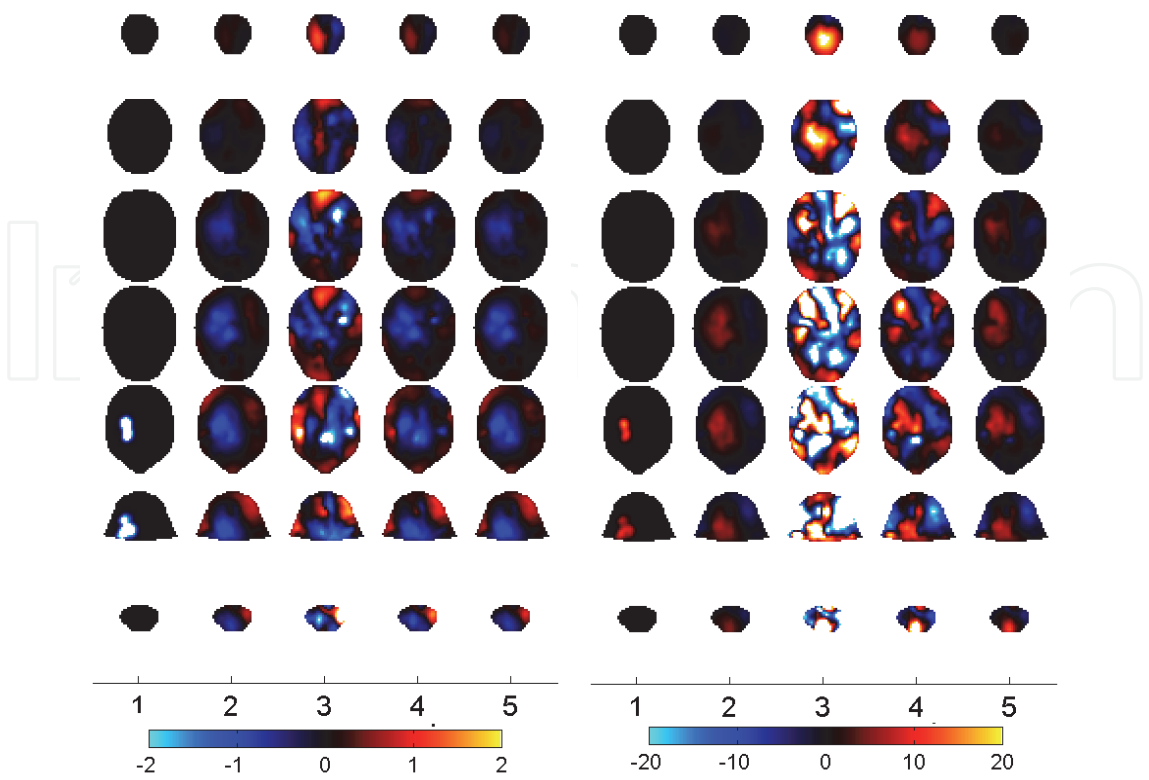
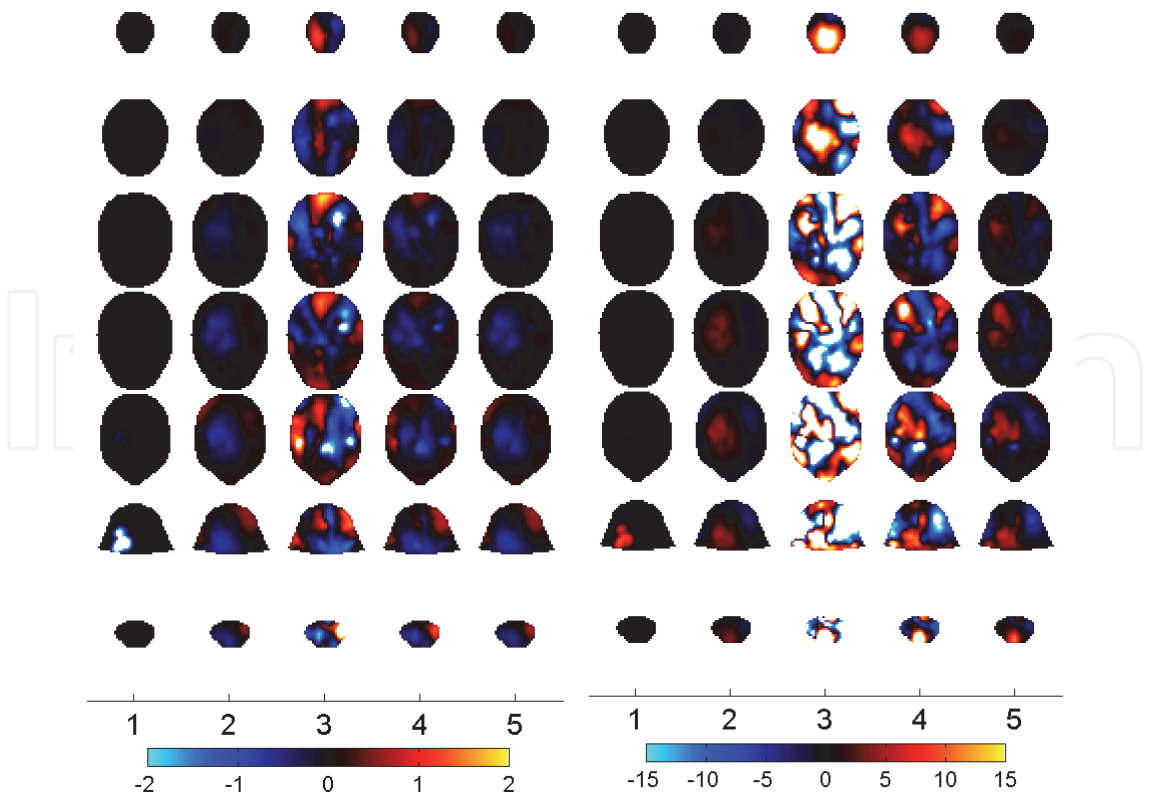Fig. 9. Parahippocampus and hippocampus together.
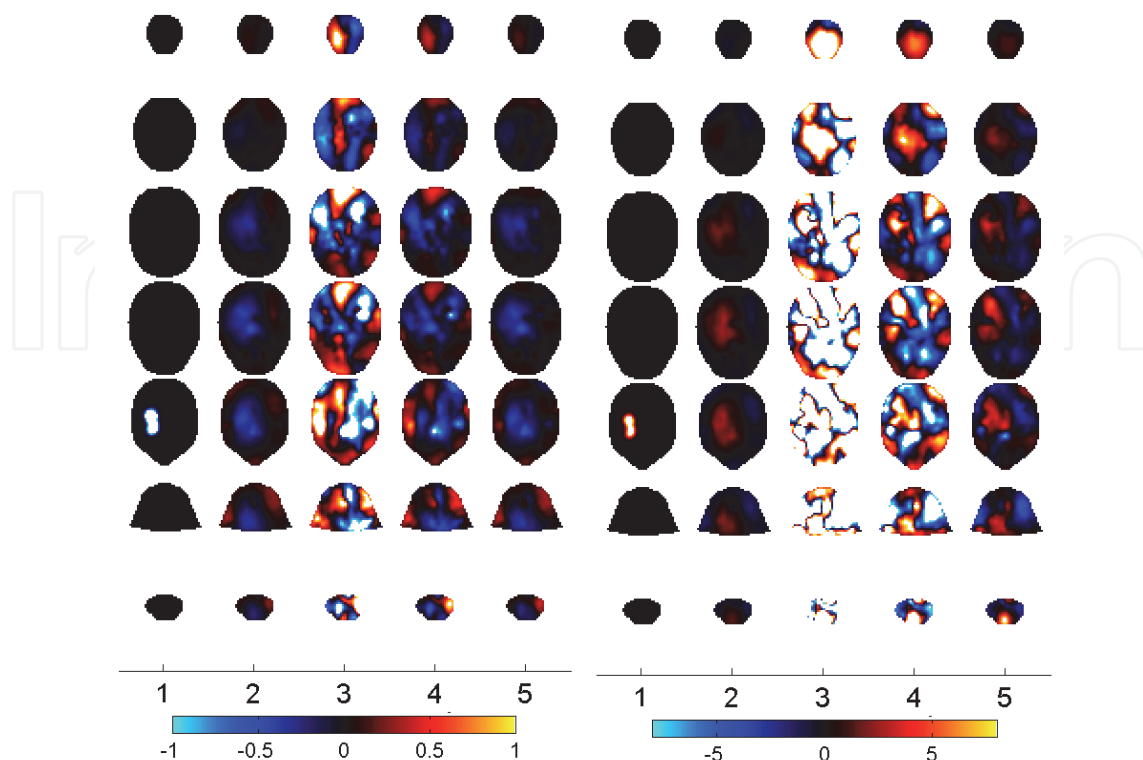

Fig. 10. Parahippocampus.

Fig. 11. Hippocampus.

5. Discussion

5.1 Summary of results

For a current level of 100 µA at all frequencies, the top 1% of the changes of the boundary voltage was almost 0.8% (1.5 µV) and 0.5% (0.6 µV) for the real and imaginary part respectively for lateral temporal lobe perturbation at 5-50 Hz. The same changes for seizures in parahippocampus and hippocampus together or separate were up to 10 times smaller. With higher current for high frequency, the top 1% of the changes of the boundary voltages was almost 1% (21 µV) and 1.4% (20 µV) for the real and imaginary part respectively for lateral temporal lobe perturbation at 50 kHz. The same changes were still up to 10 times smaller for seizures in smaller and deeper regions of the grey matter. In comparison, noise was estimated as 0.035, 0.01 or 0.002% for serial, semi-parallel or fully parallel systems respectively. With these settings, reasonably accurate images of the real component could be obtained during temporal lobe seizure for all averaging cases, and for the other three regions only for imaging with a parallel recording and injection system which permitted the most averaging. Images of the imaginary component were noisier but appeared reasonably accurate for parallel injection and recording only, and for the larger and more superficial cases of temporal lobe or combined parahippocampal and hippocampal seizures.

5.2 Technical issues

Advanced methodologies for 3D meshing, and in particular, to handle complex geometrical structures as those in the human head have been developed (Tizzard et al., 2005). These are

based on segmentation of a MRI, extrapolation and smoothing of surfaces and then meshing of the different regions of the head. This has been validated in comparison to analytical solution for a homogenous sphere (Bagshaw et al., 2003) and with experimental measurements in a homogenous spherical saline tank and humans for low frequencies (Gilad et al., 2009).

The required mesh density for modelling is affected by the following factors:

1. PDE;
2. continuity / discontinuity of the conductivity;
3. smoothness of the volume;
4. measurement error;
5. mesh quality measures;
6. linear solver and preconditioner used;
7. machine precision.

The mesh resolution adopted in the modelling presented in this chapter was chosen (by means of progressive refinement) to provide modelling errors that were below typical measurement errors. It is important to note, that the price of overly refined model is in computation and conditioning of the resulting system.

Further improvements to the accuracy of the modelling could probably be achieved by overcoming a number of other simplifications in the method presented. The conductivities of the skull, white matter, scalp and eye were represented by a unique value for each frequency. In reality they comprise more types of tissue, are not homogenously distributed, and have a different conductivity in different directions (anisotropic). The values of the conductivities of the head tissue were approximated. Considering the anisotropy of the tissues, especially for scalp and skull, may decrease the boundary voltage changes estimated up to 5 folds, as 50% more current would be shunt through the scalp (Abascal et al. 2008). Assessing the influence of anisotropy in the reconstructed images would be ideal but validation of anisotropy is mayor work in itself and was beyond the purpose of this chapter. The literature does not provide the ideal data for human head modelling, which would be given by human in-vivo 4 terminal measurements on the considered frequency range. For this reason studies that were as close as possible to this standard had to be considered and reasonable corrections and integrations between information applied. The conductivity spectra finally adopted can be considered the best approximation of the real ones within the confinements of the approximations adopted in the model and current knowledge.

The noise included in the simulated data before reconstruction was given by preliminary results and was assumed to be random. This may be worse in the case of real measurement on patients on the ward (Meeson et al., 1996) and it may not be random, and therefore not possible to reduce with averaging. This chapter presents an estimate of the minimum SNR necessary to obtain a clinically useful EIT image, but a rigorous noise characterisation is necessary.

Simulation based feasibility analysis is a powerful method as the setup of the study can be almost completely controlled and quantified. Nevertheless, modelling is obviously limited, as it is often impossible to capture adequately all the possible factors that influence the measurements. Yet, this chapter provides a general guidance for the level of hardware accuracy that is needed for application in imaging epilepsy.

5.3 Best measuring frequencies

Using the same current of 100 μA at all frequencies (in a measuring set-up where all the frequencies are injected together), recordings at the lower frequencies of 5 and 50 Hz have

the highest changes in percent and absolute values. This appears physiologically reasonable, as the greatest change in conductivity during seizures occurs at these frequencies. This is because the greatest distinction between extra- and intra-cellular space occurs at these low frequencies, being the current mostly confined outside the cell membrane.

Increasing the current according to the IEC601, the frequency with the highest changes is 50 kHz. This is because the benefit from injection of increased current appears to outweigh the larger intrinsic changes at low frequencies. This is self-evident for the criterion of absolute voltages, which may be expected to be higher as a result of the larger current injected. However, the explanation for proportional cases is not immediately apparent, as these might be expected to be independent of injected current – the standing and changed voltages during seizures might be expected to scale proportionately. The explanation is presumably because fewer voltages fall below the exclusion threshold for voltages too low to be significant, and these include those with the larger changes.

The RMS noise in the boundary voltages is about 0.3-0.4% for the real part in frequencies up to 100 kHz and it varies between 100-350% at 50 Hz and 15-25% at 50 kHz for the imaginary component. For a seizure in the temporal lobe, this translates to a signal-to-noise ratio of 2:1-3:1 for the real part measurement at 5-50 Hz with a current of 100 μA and at 50 kHz with a current of 5 mA; while for the imaginary part would be below 1:1.

Reducing the noise with averaging, it is likely that the signal-to-noise ratio could be increased 10 times at 50 kHz with a serial system or ideally more than 150 times with a fully parallel system. At this frequency the absolute value of the signal measured would be reaching tens of μV in temporal lobe epilepsy.

5.4 Noise influence on the image reconstruction

With the level of noise which is likely to be present with systems such as the UCH Mark 2.5 after averaging, only changes in the real part of the conductivity of the temporal lobe can be recognised in the reconstructed images. When the changes happen in deeper parts of the brain, the SNR is too low to give a clinically useful image. The noise is too large in the imaginary part and obscures the signal in any situation. This also suggests that if movement artefacts, which are of the order of few percent (Fabrizi et al., 2006), are present it would be not feasible to reconstruct any image. Even in the best case, the spatial resolution of the obtained EIT images is presently not alone good enough to guide the surgeon as to where to perform tissue resection. However this is likely to be at least as good as the spatial resolution of the EEG inverse source modelling (Merlet and Gotman, 2001), with which epileptic foci were identified within the resection borders in 90% of cases (Michel et al., 2004).

The SNR may be enhanced averaging more frames, but with a penalty in temporal resolution, using other signal processing tools or a different EIT system. A semi-parallel system seems to be able to image the real part of the perturbation in an area as small as the parahippocampus, but only the imaginary part of a perturbation in the temporal lobe. A fully-parallel system seems to be able to image everything, except the imaginary part for a perturbation in the hippocampus.

5.5 Future work

Sensitivity improvements rely on the possibility of reducing the baseline noise and on the intrinsic EIT instrumentation sensitivity. It may also be possible to average across different seizures in the same subject, assuming that those arising from the same onset zone can be identified clinically. Now that figures for the boundary voltage changes expected during

seizures have been estimated, researchers need to ascertain that baseline noise can be kept well below the signal under controlled and clinical conditions.

The baseline variability in previous experiments was of the order of a few percent using standard EEG electrodes and it was mostly related to movement, and was presumably due changes in contact impedance (Fabrizi et al., 2006). Alternative electrode designs, such as hydrogel electrodes, have been explored (Tidswell et al., 2003) and should be reconsidered for reducing movement artefacts under ambulatory condition. As it is already common practice in long term EEG monitoring, electrodes could also be secured with collodion, which is a kind of medical glue. Future work may include the use of signal processing tools, such as principal component analysis, already implemented in EEG, to enhance EIT sensitivity, which may separate the voltage changes of interest from the noise (Perez-Juste Abascal, 2007).

It seems possible that baseline variability can be reduced below the signal expected, especially when the seizure occurs in the temporal lobe, as this has been possible in animal studies. The first useful experiment that could be carried out in the telemetry ward would be similar to that conducted by Gilad (Gilad and Holder, 2009). Employing patients with known epileptic conditions, an array of electrodes could be placed on the side of the head where the epilepsy onset area is expected, inject current from the best current injection pair and record potential from all the other electrodes combinations without involving current injection switching. This would be the optimal set-up to measure seizure-related boundary voltage changes, whose detection would lead to a future application of EIT as new method for neuroimaging in epilepsy.

The current EIT systems designed for brain imaging are the UCH Mk 2.5 (McEwan et al., 2006) and UCH Mk1b (Yerworth et al., 2002) serial systems and the KHU Mk1, which has parallel recording capabilities (Oh et al., 2007). However the possibility of using fully-parallel EIT systems originally designed for other applications could be considered. The Dartmouth group developed a fully parallel multifrequency 64-channel system for breast imaging (10kHz to 10MHz) which has an acquisition rate of 30 fps, that could possibly be raised to 60 fps adopting only 32 channels (Halter et al., 2008). The OXBACT 5 has been developed for thoracic imaging, it has a frequency range between 26 - 56 kHz, 16 current sources, 64 voltage measurement and could acquire 25 fps (Yue and McLeod, 2008). Another system developed for thoracic imaging is the Rensselaer ACT4, which measures between 300Hz - 1MHz and has 72 channels and a slower acquisition rate of 2 fps (Liu et al., 2005). So it appears that with already available systems a noise reduction between 5 and 8 times could be obtained.

On the basis of the predictions reported in this chapter, it seems plausible that neocortical seizures could be imaged if movement artefact could be kept to a minimum. This could be achieved by recording in the quiet interval of a few seconds before clonic or tonic movement occurs. It may also be possible to improve signal-to-noise by averaging across seizures and by recording at different frequencies and employing signal processing tools which separate the signal of interest from background activities. With these manoeuvres, it may also be possible to image deeper seizures from the mesial temporal lobe or deeper sources from other regions of the brain.

6. Appendix A. Derivation of complex conductivity changes during seizures

In the following discussion these symbols were adopted:
- $\rho *^r{}_n$ (= $\rho'^r{}_n$ + j$\rho''^r{}_n$) the resistivity before the onset of the spreading depression at frequencies between 5 Hz and 50 kHz, where the superscript r indicates data recorded by Ranck (Ranck, 1963; Rank, 1964; Ranck and Bement, 1965);

- $\rho*^r_{sd}$ (= ρ'^r_{sd} +jρ''^r_{sd}) the average of the resistivity over the 30 sec with the highest changes at frequencies between 5 Hz and 50 kHz, where the superscript r indicates data recorded by Ranck (Ranck, 1963; Rank, 1964; Ranck and Bement, 1965);
- $\Delta\sigma'^y_{sd}$ the percent change in conductivity at frequencies between 300 kHz and 100 MHz, where the superscript y indicates data recorded by Yoon (Yoon et al., 1999);
- $\Delta\varepsilon^y_{sd}$ the percent change in dielectric constant at frequencies between 300 kHz and 100 MHz, where the superscript y represents Yoon measurements;
- $\Delta\rho_{ep}$ the resistivity change due to epilepsy measured at 47 kHz by Rao (Rao, 2000).

The subscript n stays indicates "normal", sd for "spreading depression" and ep for "epilepsy". The correction factor to account for the differences between spreading depression and epilepsy is calculated as:

$$R_\rho = \frac{\Delta\rho_{ep}}{\Delta\rho''^r_{sd}} \quad \text{where} \quad \Delta\rho''^r_{sd} = \frac{\rho''^r_{sd}(50kHz) - \rho''^r_n(50kHz)}{\rho''^r_n(50kHz)}$$

The resistivity during epilepsy at frequencies between 5 Hz and 50 kHz can be estimated as:

$$\rho'^r_{ep} = (\rho'^r_{sd} - \rho'^r_n)R_\rho + \rho'^r_n$$
$$\rho''^r_{ep} = (\rho''^r_{sd} - \rho''^r_n)R_\rho + \rho''^r_n$$

And the conductivity for normal, spreading depression and epileptic conditions as:

$$\sigma'^r_n = \frac{\rho'^r_n}{\rho'^{r2}_n + \rho''^{r2}_n} \quad \sigma'^r_{ep} = \frac{\rho'^r_{ep}}{\rho'^{r2}_{ep} + \rho''^{r2}_{ep}}$$

$$\sigma''^r_n = \frac{\rho''^r_n}{\rho'^{r2}_n + \rho''^{r2}_n} \quad \sigma''^r_{ep} = \frac{\rho''^r_{ep}}{\rho'^{r2}_{ep} + \rho''^{r2}_{ep}}$$

The percentage changes in conductivity at frequencies between 5 Hz and 50 kHz are then:

$$\Delta\sigma'^r_{ep} = \frac{\sigma'^r_{ep} - \sigma'^r_n}{\sigma'^r_n}$$

$$\Delta\sigma''^r_{ep} = \frac{\sigma''^r_{ep} - \sigma''^r_n}{\sigma''^r_n}$$

To translate the percent change of the conductivity at frequencies between 300 kHz and 100 MHz due to spreading depression in percent change due to epilepsy another conversion factor has to be calculated:

$$R_\sigma = \frac{\Delta\sigma'^r_{ep}(50kHz)}{\Delta\sigma'^r_{sd}(50kHz)}$$

Therefore the conductivity changes due to epilepsy at frequencies between 300 kHz and 100 MHz are:

$$\Delta\sigma'^y_{ep} = R_\sigma \Delta\sigma'^y_{sd}$$

A percent change in the dielectric constant corresponds with a percent change in the quadrature component of the conductivity, therefore:

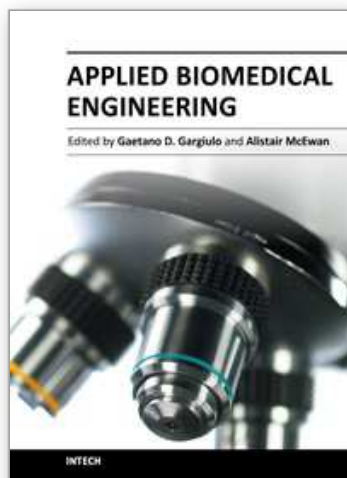$$\Delta\sigma''^y_{ep} = R_\sigma \Delta\varepsilon^y_{sd}$$

The overall spectrum of the percent conductivity change was obtained by joining $\Delta\sigma'^r_{ep}$ with $\Delta\sigma'^y_{ep}$ and $\Delta\sigma''^r_{ep}$ with $\Delta\sigma''^y_{ep}$ and used to modify the grey matter conductivity to simulate epileptic conditions (Fig. 2).

7. References

Bagshaw, A.P., Liston, A.D., Bayford, R.H., Tizzard, A., Gibson, A.P., Tidswell, A.T., Sparkes, M.K., Dehghani, H., Binnie, C.D., Holder, D.S., 2003. Electrical impedance tomography of human brain function using reconstruction algorithms based on the finite element method. Neuroimage. 20, 752-764.

Baumann, S.B., Wozny, D.R., Kelly, S.K., Meno, F.M., 1997. The electrical conductivity of human cerebrospinal fluid at body temperature. IEEE Trans.Biomed.Eng 44, 220-223.

Boone, K., Lewis, A.M., Holder, D.S., 1994. Imaging of cortical spreading depression by EIT: implications for localization of epileptic foci. Physiol Meas. 15 Suppl 2a, A189-A198.

Elazar, Z., KADO, R.T., Adey, W.R., 1966. Impedance changes during epileptic seizures. Epilepsia 7, 291-307.

Engel, J., Jr., 1993. Update on surgical treatment of the epilepsies. Summary of the Second International Palm Desert Conference on the Surgical Treatment of the Epilepsies (1992). Neurology 43, 1612-1617.

Fabrizi, L., Sparkes, M., Horesh, L., Perez-Juste Abascal, J.F., McEwan, A., Bayford, R.H., Elwes, R., Binnie, C.D., Holder, D.S., 2006. Factors limiting the application of Electrical Impedance Tomography for identification of regional conductivity changes using scalp electrodes during epileptic seizures in humans. Physiol.Meas. 27, 163-174.

Foster, K.R., Schwan, H.P., 1989. Dielectric properties of tissues and biological materials: a critical review. Crit Rev.Biomed.Eng 17, 25-104.

Fox, J.E., Bikson, M., Jefferys, J.G., 2004. Tissue resistance changes and the profile of synchronized neuronal activity during ictal events in the low-calcium model of epilepsy. J.Neurophysiol. 92, 181-188.

Gabriel, S., Lau, R.W., Gabriel, C., 1996a. The dielectric properties of biological tissues: II. Measurements in the frequency range 10 Hz to 20 GHz. Phys.Med.Biol. 41, 2251-2269.

Gabriel, S., Lau, R.W., Gabriel, C., 1996b. The dielectric properties of biological tissues: III. Parametric models for the dielectric spectrum of tissues. Phys.Med.Biol. 41, 2271-2293.

Gilad, O., Holder, D.S., 2009. Impedance changes recorded with scalp electrodes during visual evoked responses: implications for Electrical Impedance Tomography of fast neural activity. Neuroimage. 47, 514-522.

Gilad, O., Horesh, L., Holder, D.S., 2009. A modelling study to inform specification and optimal electrode placement for imaging of neuronal depolarization during visual evoked responses by electrical and magnetic detection impedance tomography. Physiol Meas. 30, S201-S224.

Halter, R.J., Hartov, A., Paulsen, K.D., 2008. A broadband high-frequency electrical impedance tomography system for breast imaging. IEEE Trans.Biomed.Eng 55, 650-659.

Holder, D.S., 2005. Electrical Impedance Tomography. Insitute of Physics Publishing, Bristol and Philadelphia.

Horesh, L., 2006. Some novel approaches in modelling and image reconstruction for multi-frequency electrical impedance tomography of the human brain. University College London, London.

Kosterich, J.D., Foster, K.R., Pollack, S.R., 1983. Dielectric permittivity and electrical conductivity of fluid saturated bone. IEEE Trans.Biomed.Eng 30, 81-86.

Latikka, J., Kuurne, T., Eskola, H., 2001. Conductivity of living intracranial tissues. Phys.Med.Biol. 46, 1611-1616.

Leao, A.A.P., 1944. Spreading depression of activity in cerebral cortex. J.Neurophysiol. 7, 359-390.

Lindenblatt, G., Silny, J., 2001. A model of the electrical volume conductor in the region of the eye in the ELF range. Phys.Med Biol 46, 3051-3059.

Liu, N., Saulnier, G.J., Newell, J.C., Kao, T.J., 2005. ACT 4: A high-precision, multi-frequency Electrical Impedance Tomograph. XI Conf. on Biomedical application of EIT (London, UK).

Lux, H.D., Heinemann, U., Dietzel, I., 1986. Ionic changes and alterations in the size of the extracellular space during epileptic activity. Adv.Neurol. 44, 619-639.

McEwan, A., Romsauerova, A., Yerworth, R., Horesh, L., Bayford, R., Holder, D., 2006. Design and calibration of a compact multi-frequency EIT system for acute stroke imaging. Physiol Meas. 27, S199-S210.

Meeson, S., Blott, B.H., Killingback, A.L., 1996. EIT data noise evaluation in the clinical environment. Physiol Meas. 17 Suppl 4A, A33-A38.

Merlet, I., Gotman, J., 2001. Dipole modeling of scalp electroencephalogram epileptic discharges: correlation with intracerebral fields. Clin.Neurophysiol. 112, 414-430.

Michel, C.M., Murray, M.M., Lantz, G., Gonzalez, S., Spinelli, L., Grave de, P.R., 2004. EEG source imaging. Clin.Neurophysiol. 115, 2195-2222.

Oh, T.I., Lee, E.J., Woo, E.J., Kwon, O., Seo, J.K., 2005. Multi-frequency EIT and TAS hardware development. XI Conf. on Biomedical application of EIT (London, UK).

Oh, T.I., Woo, E.J., Holder, D., 2007. Multi-frequency EIT system with radially symmetric architecture: KHU Mark1. Physiol Meas. 28, S183-S196.

Perez-Juste Abascal, J.F., 2007. Improvement in reconstruction algorithms for electrical impedance tomography of brain function. University College London.

Polydorides, N., Lionheart, W.R.B., 2002. Toolkit for three-dimensional Electrical Impedance Tomography: a contribution to the Electrical Impedance Tomography and Diffuse Optical Reconstruction software project. Mea.Sci.Technol. 13, 1871-1883.

Ranck Jr, J.B., 1964. Specific impedance of cerebral cortex during spreading depression, and an analysis of neuronal, neuroglial, and interstitial contributions. Exp.Neurol. 9, 1-16.

Ranck, J.B., Jr., 1963. Analysis of specific impedance of rabbit cerebral cortex. Exp.Neurol. 7, 153-174.

Ranck, J.B., Jr., BEMENT, S.L., 1965. The specific impedance of the dorsal columns of cat: an anisotropic medium. Exp.Neurol. 11, 451-463.

Rao, A., 2000. Electrical Impedance Tomography of brain activity: studies into its accuracy and physiological mechanisms. London: University College London.

Rosenow, F., Luders, H., 2001. Presurgical evaluation of epilepsy. Brain 124, 1683-1700.

Sierpowska, J., Hakulinen, M.A., Toyras, J., Day, J.S., Weinans, H., Jurvelin, J.S., Lappalainen, R., 2005. Prediction of mechanical properties of human trabecular bone by electrical measurements. Physiol Meas. 26, S119-S131.

Sierpowska, J., Toyras, J., Hakulinen, M.A., Saarakkala, S., Jurvelin, J.S., Lappalainen, R., 2003. Electrical and dielectric properties of bovine trabecular bone--relationships with mechanical properties and mineral density. Phys.Med.Biol. 48, 775-786.

Soni, N.K., Paulsen, K.D., Dehghani, H., Hartov, A., 2006. Finite element implementation of Maxwell's equations for image reconstruction in electrical impedance tomography. IEEE Trans.Med Imaging 25, 55-61.

Tidswell, A.T., Bagshaw, A.P., Holder, D.S., Yerworth, R.J., Eadie, L., Murray, S., Morgan, L., Bayford, R.H., 2003. A comparison of headnet electrode arrays for electrical impedance tomography of the human head. Physiol Meas. 24, 527-544.

Tizzard, A., Horesh, L., Yerworth, R.J., Holder, D.S., Bayford, R.H., 2005. Generating accurate finite element meshes for the forward model of the human head in EIT. Physiol Meas. 26, S251-S261.

Van Harreveld, A., Shade, J.P., 1962. Changes in the electrical conductivity of cerebral cortex during seizure activity. Exp.Neurol. 5, 383-400.

Yerworth, R.J., Bayford, R.H., Cusick, G., Conway, M., Holder, D.S., 2002. Design and performance of the UCLH mark 1b 64 channel electrical impedance tomography (EIT) system, optimized for imaging brain function. Physiol Meas. 23, 149-158.

Yoon, R.S., Czaya, A., Kwan, H.C., Joy, M.L., 1999. Changes in the complex permittivity during spreading depression in rat cortex. IEEE Trans.Biomed.Eng 46, 1330-1338.

Yue, X., McLeod, C., 2008. FPGA design and implementation for EIT data acquisition. Physiol Meas. 29, 1233-1246.

Applied Biomedical Engineering

Edited by Dr. Gaetano Gargiulo

This book presents a collection of recent and extended academic works in selected topics of biomedical technology, biomedical instrumentations, biomedical signal processing and bio-imaging. This wide range of topics provide a valuable update to researchers in the multidisciplinary area of biomedical engineering and an interesting introduction for engineers new to the area. The techniques covered include modelling, experimentation and discussion with the application areas ranging from bio-sensors development to neurophysiology, telemedicine and biomedical signal classification.

How to reference

In order to correctly reference this scholarly work, feel free to copy and paste the following:

INTECH
open science | open minds